Chemical Science

ROYAL SOCIETY OF CHEMISTRY

EDGE ARTICLE

View Article Online
View Journal | View Issue

Cite this: *Chem. Sci.*, 2026, **17**, 1127

All publication charges for this article have been paid for by the Royal Society of Chemistry

Macrocyclic geminal diols: synthesis, structures, stability and photophysical properties†

Bo Zou,[a] Xiaolin Chen,[a] Haoran Liu,[a] Sijie Wen,[a] Jieqing Huang,[a] Hengshan Wei,[a] Jinqing Huang,[b] Yucheng Gu,[c] Bingjia Xu,*[d] Jun Fan*[a] and Hua-Wei Jiang*[a]

Geminal diols are generally unstable and prone to dehydration, yielding carbonyl compounds and making their isolation as discrete species highly challenging. Herein, we report the synthesis, structural characterization, and stability of a series of crystalline, stable, and rigid macrocyclic *gem*-diols obtained *via* acid hydrolysis of macrocyclic ketal precursors at −25 °C. Single-crystal X-ray diffraction analysis of these compounds reveals O–C–O bond angles of approximately 111°, along with extensive hydrogen-bonding networks that contribute to stabilizing the *gem*-diols. Thermogravimetric and hydrolytic analyses reveal a pronounced size-dependent stability trend. Theoretical calculations indicate that the enhanced stability of smaller *gem*-diol macrocycles stems from their ability to relieve substantial angle strain *via* sp^3 hybridization at the methylene carbon, an effect that diminishes as ring size increases. Based on our experimental and computational results, the inner angle value of the macrocyclic ketone is proposed as a criterion for evaluating the relative stability of macrocyclic ketones *versus* their *gem*-diol forms. The photophysical properties of the macrocyclic geminal diols and macrocyclic diketones are also examined. This work broadens the scope of stable geminal diols and provides fundamental insights into their structure–stability relationships, thereby laying the groundwork for the strategic design and synthesis of structurally diverse macrocyclic geminal diols.

Received 23rd October 2025
Accepted 11th November 2025

DOI: 10.1039/d5sc08216a

rsc.li/chemical-science

Introduction

A geminal diol (*gem*-diol) is defined as a diol in which two hydroxyl groups are bonded to the same carbon atom. These species are recognized as key intermediates in a variety of organic and biochemical transformations,[1–5] as well as in atmospheric processes,[6–8] and they hold considerable potential for applications in organic synthesis,[9] environmental chemistry,[10] biochemistry,[11,12] and coordination chemistry.[13–20] *gem*-Diols readily undergo dehydration to yield carbonyl compounds, making them generally difficult to isolate (Fig. 1a). For example, methanediol—the simplest geminal diol—although known to exist predominantly as a stable species in equilibrium with formaldehyde in aqueous solution,[21] was not successfully isolated in the gas phase until 2022 by Kaiser *et al.*[22] The stability of geminal diols is primarily influenced by steric hindrance, hydrogen bonding, strong electron-withdrawing effects, and ring strain.[23–27] For instance, acetone forms its hydrate less readily than formaldehyde owing to steric hindrance,[21] while chloral hydrate[28] and ninhydrin hydrate[29] are stabilized by strong electron-withdrawing groups. Although ring strain is recognized as an important contributor to the stability of geminal diols, only a limited number of strain-stabilized examples have been reported to date. 1,1-Cyclopropanediol, the smallest cyclic diol, can be synthesized *via* hydration of cyclopropenone,[30,31] and its stability is attributed to the substantial angle strain of the three-membered ring, which enables its isolation as a stable compound.[21,23] However, 1,1-cyclobutanediol, 1,1-cyclopentanediol, and 1,1-cyclohexanediol can only be formed in small amounts at equilibrium with their corresponding ketones and water (Fig. 1b).[21,32] Additionally, coordination of a metal ion to certain polycyclic compounds can increase strain and promote *gem*-diol formation.[33,34] Recent years have witnessed substantial progress in the synthesis of strained macrocyclic organic compounds.[35–50] Macrocyclic organic compounds, in contrast to aliphatic small-ring analogues, exhibit greater structural diversity and offer enhanced potential for rational design and functional modification. Therefore, investigating the synthesis, structures, and

[a]*School of Chemistry, South China Normal University, Guangzhou 510006, China. E-mail: fanj@scnu.edu.cn; hwjiang@m.scnu.edu.cn*

[b]*Department of Chemistry, The Hong Kong University of Science and Technology, Clear Water Bay, Kowloon, Hong Kong, China*

[c]*Syngenta Jealott's Hill International Research Centre, Bracknell, Berkshire, UK*

[d]*School of Environmental and Chemical Engineering, Wuyi University, Jiangmen, 529020, China. E-mail: bingjiaxu@m.scnu.edu.cn*

† On the auspicious occasion of her 95th birthday, this paper is dedicated to Professor Youyou Tu, the esteemed recipient of the 2015 Nobel Prize in Physiology or Medicine, in recognition of her groundbreaking discovery of Artemisinin, which has saved millions of lives worldwide.

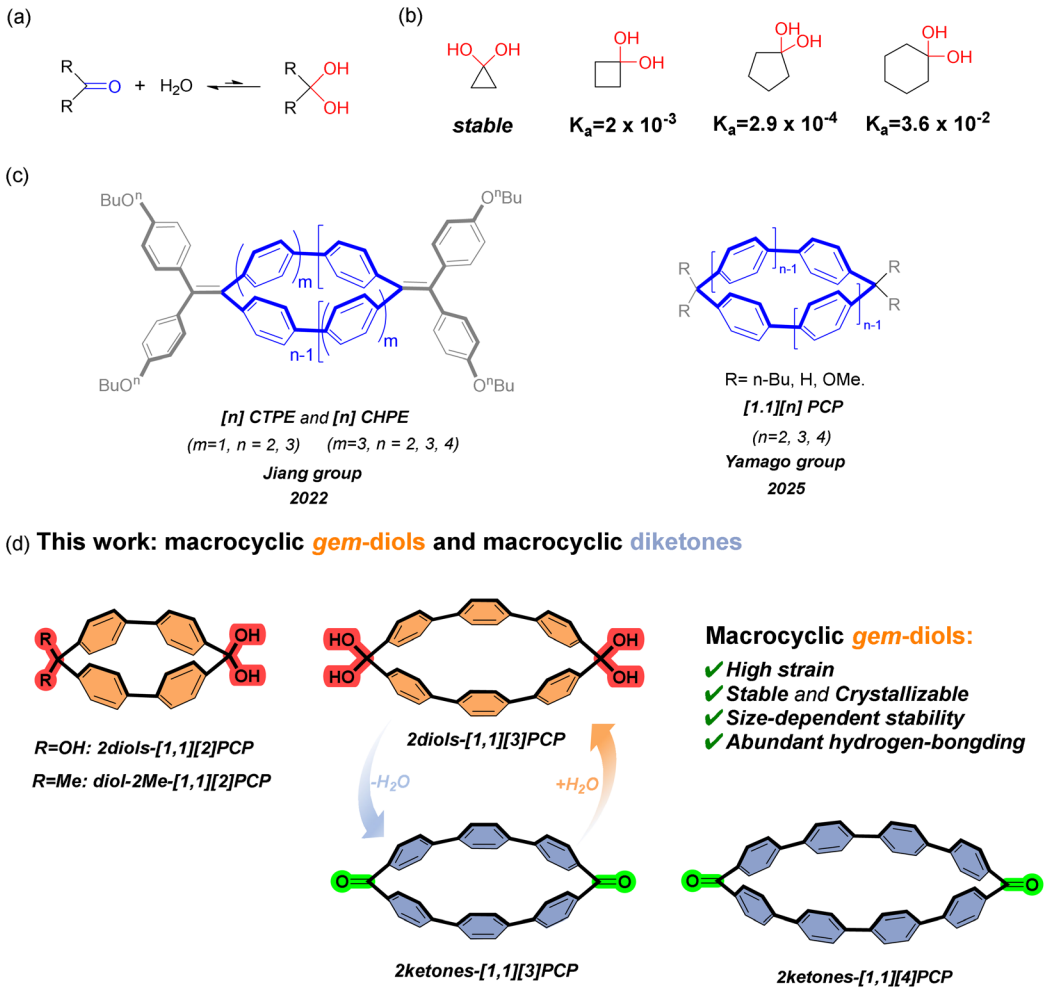

Fig. 1 (a) The reversible hydration equilibrium between carbonyl compounds and geminal diols. (b) 1,1-Cyclopropanediol, 1,1-cyclobutanediol, 1,1-cyclopentanediol and 1,1-cyclohexanediol, along with their dehydration equilibrium constants. (c) Reported examples of macrocyclic framework. (d) Structures of **2diols-[1,1][2]PCP**, **2diols-[1,1][3]PCP**, **2ketones-[1.1][3]PCP**, **2ketones-[1.1][4]PCP** and **diol-2Me-[1,1][2]PCP**.

stability of strained macrocyclic diols is of considerable interest.

We previously accessed two series of rigid porphyrin wheel β–β connected and biphenylene-linked—*via* platinum-mediated cyclization, with the highest strain energies of each series reaching 77.4 kcal mol^{-1} and 49.3 kcal mol^{-1}, respectively.[51,52] One-dimensional porphyrin nanotubes were also constructed *via* hydrogen-bond-driven self-assembly of porphyrin wheels bearing carboxylic acid groups.[53] In 2022, we first reported [*n*]CTPE and [*n*]CHPE—two rigid macrocycles composed of *para*-biphenyl units and ylidene linkers (Fig. 1c, left).[54] [2]CTPE exhibited distinctive dual-state emission properties and a long solid-state fluorescence lifetime, whereas larger macrocycles displayed enhanced aggregation-induced emission relative to the TPE monomer, indicating size-dependent physicochemical behavior. We subsequently made considerable efforts to synthesize analogous biphenylene macrocycles with varied bridging units. During this period, in 2025, the Yamago group reported similar rigid macrocycles, [1.1][*n*]paracyclophanes ([1,1][*n*]PCPs) (Fig. 1c, right),[55] composed of *para*-biphenyl units connected by methylene bridges, and confirmed the presence of through-space conjugation between biphenyl units within the macrocycles. Here, we report the synthesis of macrocyclic *gem*-diols (**2diols-[1.1][2]PCP**, **2diols-[1.1][3]PCP**, **diol-2Me-[1.1][2]PCP**) *via* hydrolysis of the corresponding ketal precursors (**2ketals-[1.1][2]PCP**, **2ketals-[1.1][3]PCP**, **2ketals-[1.1][4]PCP**, **ketal-2Me-[1.1][2]PCP**). The structures of these macrocyclic *gem*-diols, as well as two macrocyclic diketones (**2ketones-[1.1][3]PCP**, **2ketones-[1.1][4]PCP**), were elucidated. The thermal stability of these macrocyclic *gem*-diols was investigated using thermogravimetric analysis (TGA) and further evaluated through theoretical calculations.

Results and discussion

Synthesis of macrocyclic *gem*-diols and macrocyclic diketones

The precursors of the 2ketals-[1.1][*n*]PCPs were synthesized through platinum-mediated cyclization followed by reductive elimination (see SI). The macrocyclic *gem*-diol **2diols-[1.1][2]**

Table 1 Dehydration of 2diols-[1,1][2]PCP [a]

Entry	Temp.	Time	Yield [b] of 2diols-[1.1][2]PCP	Yield [b] of 1
1	−25 °C	30 min	96% (78%)[c]	4%
2	0 °C	30 min	87%	13%
3	25 °C	30 min	43%	57%
4	70 °C	30 min	0%	100%

[a] All the reactions were carried out using **2ketals-[1.1][2]PCP** (20 mg, 0.04 mmol) and trifluoroacetic acid (3 ml). [b] Determined by ^{1}H NMR spectroscopy unless otherwise noted. [c] Isolated yield.

PCP was synthesized by subjecting **2ketals-[1.1][2]PCP** to an excess of trifluoroacetic acid (TFA) (Table 1). After complete conversion of **2ketals-[1.1][2]PCP**, the acid was neutralized with a saturated aqueous sodium bicarbonate solution. The resulting mixture was filtered, and the crude product was recrystallized to yield the pure macrocyclic *gem*-diol. The acid hydrolysis conditions were optimized using **2ketals-[1.1][2]PCP** as a model compound. It was found that TFA proved to be a suitable acid for the efficient hydrolysis of **2ketals-[1.1][2]PCP**. Parallel reactions were performed over 30 minutes at 70 °C, 25 °C, 0 °C, and −25 °C (Table 1), and yields were determined by ^{1}H NMR spectroscopy. At 70 °C, the desired *gem*-diol product was not obtained; instead, the starting material was completely converted into the ring-opening product **1**, identified as 4′-([1,1′-biphenyl]-4-carbonyl)-[1,1′-biphenyl]-4-carboxylic acid. At 25 °C, the desired **2diols-[1.1][2]PCP** was obtained in 43% yield together with product **1** in 57% yield, whereas at 0 °C, the yield of **2diols-[1.1][2]PCP** increased to 87%, with 13% of **1** formed. At −25 °C,the desired product was obtained in 96% yield, with only 4% of **1** observed. The reaction time also affected the product distribution. Thin-layer chromatography showed incomplete conversion at 20 min, while full conversion was achieved at 30 min with the highest yield of **2diols-[1.1][2]PCP**. Prolonged reaction times led to increased formation of byproduct **1**. Thus, TFA at −25 °C for 30 min was selected as the optimal condition for hydrolysis, affording **2diols-[1.1][2]PCP** in 78% isolated yield after recrystallization. The hydrolysis of **2dbts-[1.1][2]PCP**, in which methylene carbons are connected to 1,4-dioxabutan-1,4-diyl units, did not proceed under the optimized conditions, likely due to the enhanced stability of the five-membered rings (see SI).

Acid hydrolysis of the macrocyclic ketal precursors **2ketals-[1.1][3]PCP** and **ketal-2Me-[1.1][2]PCP** under the optimized conditions afforded **2diols-[1.1][3]PCP** and **diol-2Me-[1.1][2]PCP** in isolated yields of 79% and 58%, respectively (Scheme 1a and 1c). However, hydrolysis of **2ketals-[1.1][4]PCP** afforded the macrocyclic diketone **2ketones-[1.1][4]PCP** in 80% isolated yield, and no *gem*-diol product was detected (Scheme 1b). The transformation of **2diols-[1.1][2]PCP** and **2diols-[1.1][3]PCP** into their respective ketone counterparts was then attempted by heating in toluene under reflux for 5 h. While **2diols-[1.1][2]PCP** remained unchanged, **2diols-[1.1][3]PCP** was successfully converted into **2ketones-[1.1][3]PCP** (78% isolated yield) (Scheme 1a). The characterization data of **2ketones-[1.1][3]PCP** were consistent with those reported by Yamago group.[56]

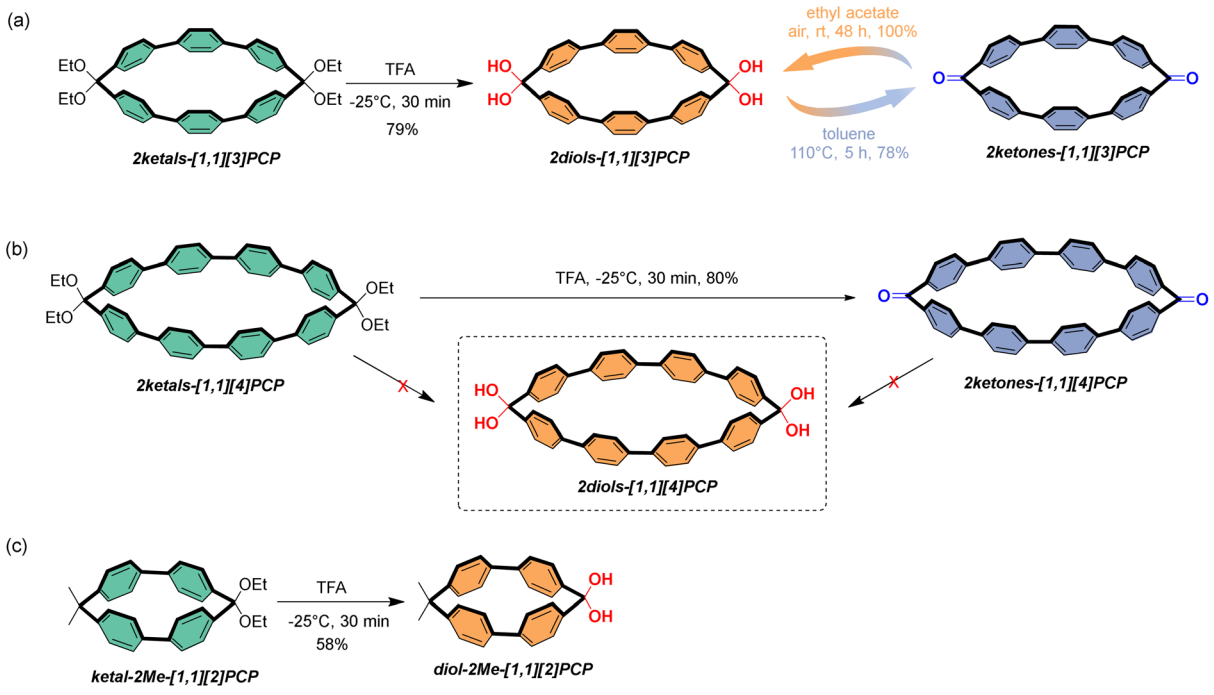

Scheme 1 Synthesis of (a) 2diols-[1,1][3]PCP and 2ketones-[1,1][3]PCP, (b) 2ketones-[1,1][4]PCP (c) diol-2Me-[1,1][2]PCP.

Interestingly, when the ethyl acetate solution of **2ketones-[1.1][3]PCP** was exposed to ambient air for 48 h, it quantitatively reverted to **2diols-[1.1][3]PCP** (Scheme 1a). In contrast, **2ketones-[1.1][4]PCP** remained unchanged under identical conditions (Scheme 1b).

Structure of macrocyclic *gem*-diols and macrocyclic diketones

The ^{1}H NMR spectra of **2diols-[1.1][2]PCP** and **diol-2Me-[1.1][2]PCP** each exhibited a singlet at $\delta = 6.86$ ppm, attributable to the geminal diol protons (see SI, Fig. S1a and S1c). The geminal diol carbon in both compounds appeared at $\delta = 97.48$ ppm in the ^{13}C NMR spectrum (see SI, Fig. S32 and S36). For **2diols-[1.1][3]PCP**, a similar singlet appeared at $\delta = 6.96$ ppm in the ^{1}H NMR spectrum (see SI, Fig. S1b), and the corresponding carbon resonance was detected at $\delta = 96.64$ ppm in the ^{13}C NMR spectrum. In contrast, the ^{13}C NMR spectra of **2ketones-[1.1][3]PCP** and **2ketones-[1.1][4]PCP** exhibited resonances at $\delta = 201.06$ ppm and $\delta = 200.83$ ppm, respectively, which were assigned to the carbonyl carbons. MALDI-TOF mass spectra of the three macrocyclic geminal diols (**2diols-[1.1][2]PCP**, **2diols-[1.1][3]PCP**, and **diol-2Me-[1.1][2]PCP**) and two macrocyclic diketones (**2ketones-[1.1][3]PCP** and **2ketones-[1.1][4]PCP**) showed molecular ion peaks at $m/z = 396.138$, $m/z = 548.158$, $m/z = 392.176$, $m/z = 513.138$ and $m/z = 664.247$, in agreement with their calculated values of $C_{26}H_{20}O_4^+$ $[M]^+$: 396.136, $C_{38}H_{28}O_4^+$ $[M + H]^+$: 548.199, $C_{28}H_{24}O_2^+$ $[M]^+$: 392.178, $C_{38}H_{25}O_2^+$ $[M + H]^+$: 513.184 and $C_{50}H_{32}O_2^+$ $[M]^+$: 664.240, respectively.

To gain further insight into the structural characteristics of these macrocyclic geminal diols, single crystals were grown of **2diols-[1.1][2]PCP**, **2diols-[1.1][3]PCP**, and **diol-2Me-[1.1][2]PCP**, as well as the macrocyclic diketone **2ketones-[1.1][4]PCP** and the ketal precursors **ketal-2Me-[1.1][2]PCP**, **2ketals-[1.1][2]PCP**, **2ketals-[1.1][3]PCP**, and **2ketals-[1.1][4]PCP**. Their structures were unambiguously confirmed by single-crystal X-ray diffraction analysis (Fig. 2).

Each molecule exhibited an elliptical cavity, with the cavity size increasing as the ring size expanded. The exocyclic O–C–O bond angle (α_1) in **2diols-[1.1][2]PCP** (111.74°) is slightly larger than that in **2diols-[1.1][3]PCP** (110.55°), whereas the endocyclic C–C–C angle (α_2) in **2diols-[1.1][2]PCP** (101.20°) is about 3° smaller than that in **2diols-[1.1][3]PCP** (104.03°), indicating greater angular strain in the former due to its more constrained ring size. The α_2 in **2diols-[1.1][2]PCP** and **2diols-[1.1][3]PCP** are close to those observed in **2ketals-[1.1][2]PCP** (101.11°) and **2ketals-[1.1][3]PCP** (103.44°), suggesting that the overall macrocyclic strain remains nearly unchanged before and after hydrolysis. For **2diols-[1.1][2]PCP**, **2diols-[1.1][3]PCP**, and **diol-2Me-[1.1][2]PCP**, the C–O bond lengths of the geminal hydroxyl groups (1.41–1.42 Å) are longer than those in hexafluoroacetone hydrate (1.38 Å), confirming that the stabilization of these macrocyclic geminal diols arises from ring strain rather than electron effects.[57] In **diol-2Me-[1.1][2]PCP**, the intramolecular O···O distance (2.33 Å) and exocyclic O–C–O angle (111.05°) are nearly identical to those in **2diols-[1.1][2]PCP**, indicating that despite its lower symmetry, the geminal diol geometry remains essentially unchanged.

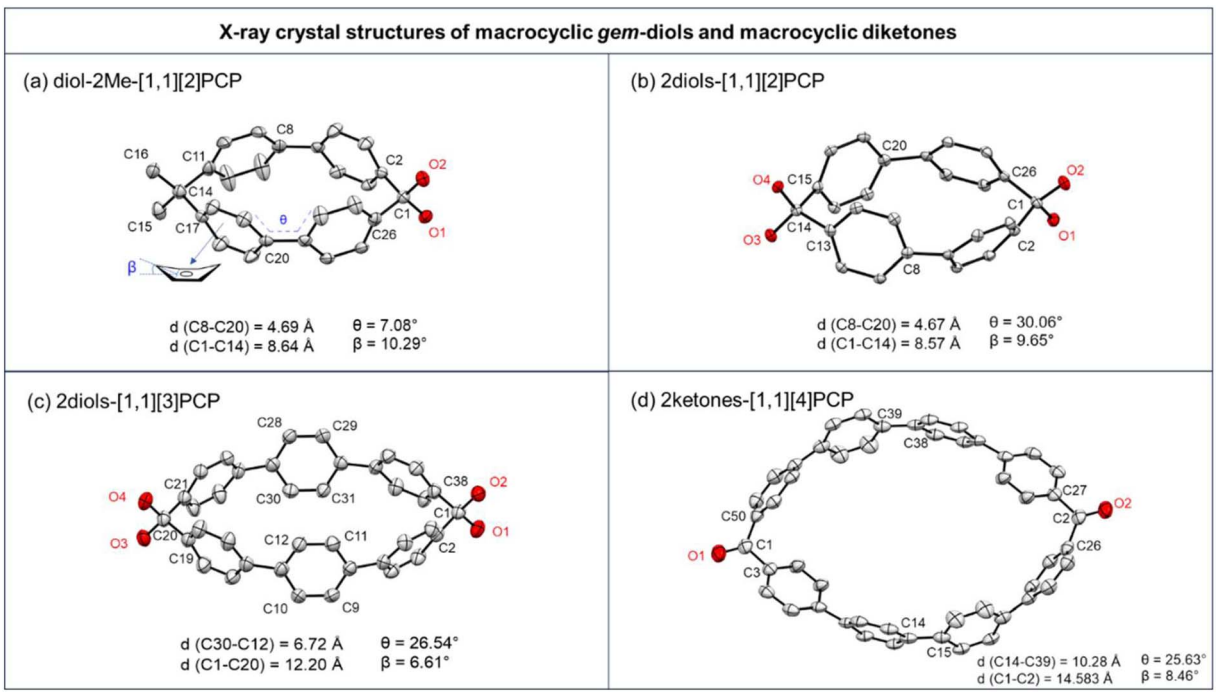

Fig. 2 X-ray crystal structures of macrocyclic *gem*-diols (a) **diol-2Me-[1,1][2]PCP**, (b) **2diols-[1,1][2]PCP**, (c) **2diols-[1,1][3]PCP**, and macrocyclic diketones (d) **2ketones-[1,1][4]PCP**. Carbon atoms are numbered in black according to the molecular symmetry. Hydrogen atoms and solvents are omitted for clarity. The thermal ellipsoids are scaled at the 50 % probability level. The average bending angles of the phenyls are defined as β. The average torsion angles are defined as θ.

Geminal diols can easily form hydrogen bonds with solvent molecules,[58] which may contribute to their stabilization. Extensive hydrogen-bonding networks are observed in the macrocyclic geminal diol **2diols-[1.1][2]PCP** (Fig. 3a). The hydroxyl groups of the geminal diol moieties form eight-membered ring structures through intermolecular hydrogen bonding with adjacent macrocycles. In addition, one hydroxyl hydrogen of the geminal diol moiety forms a hydrogen bond with an oxygen atom of the solvent molecule dimethyl sulfoxide. These intermolecular hydrogen bonds (O(1)–H(1)···O(2′) and O(1′)–H(1′)···O(2)) exhibit identical O···O distances of 2.74 Å. Hydrogen bonds are observed between **2diols-[1.1][2]PCP** and dimethyl sulfoxide solvent molecules, with O···O distances of 2.64 Å (O(2)–H(2)···O(5) and O(2′) –H(2′)···O(5′)). Similar hydrogen-bonding networks are also observed in **2diols-[1.1][3]PCP** and **diol-2Me-[1.1][2]PCP** (Fig. 3b and c). It is worth mentioning that while **2diols-[1.1][2]PCP** contains two geminal diol moieties, **diol-2Me-[1.1][2]PCP** contains only one. As a result, the density of the hydrogen-bonding network in **diol-2Me-[1.1][2]PCP** is lower, which may contribute to its reduced structural stability compared to **2diols-[1.1][2]PCP**.

For the macrocyclic diketone **2ketones-[1.1][4]PCP**, the distance between the oxygen atom and its closest carbon atom is 1.22 Å, consistent with a typical carbonyl double bond. The bond angles C(3)–C(1)–C(50) and C(26)–C(2)–C(27) are 112.84° and 113.19°, respectively, which are significantly smaller than the corresponding angle in benzophenone (116.90°),[59] indicating considerable ring strain. Upon conversion from **2ketals-[1.1][4]PCP** to **2ketones-[1.1][4]PCP**, the hybridization of the bridging carbon changes from sp^3 to sp^2 due to the formation of carbonyl groups. This transformation leads to a substantial increase in the biphenyl dihedral angle α from 106.01° to 112.92°, as well as an increase in the bending angle β of the internal phenyl units from 5.47° to 8.46°. These changes indicate that the elliptical cavity of **2ketones-[1.1][4]PCP** has a smaller eccentricity than that of **2ketals-[1.1][4]PCP**, suggesting that **2ketones-[1.1][4]PCP** accommodates greater ring strain (Table 2).

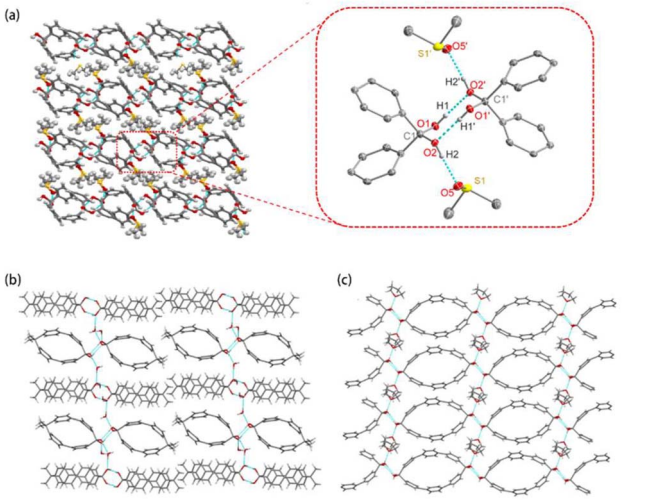

Fig. 3 (a) Hydrogen-bonded network with eight-membered ring structures in **2diols-[1,1][2]PCP**·2DMSO and the thermal ellipsoids are scaled at the 50 % probability level. Hydrogen-bonded network of (b) **diol-2Me-[1,1][2]PCP**·H_2O and (c) **2diols-[1,1][3]PCP**·2THF.

Table 2 X-ray single-crystal diffraction data of macrocyclic compounds

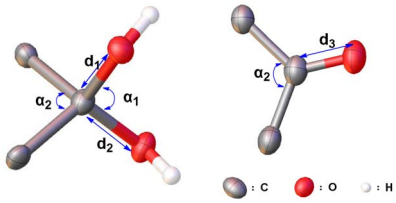

Compound	d_1[a] (Å)	d_2[b] (Å)	d_3[c] (Å)	α_1[d] (°)	α_2[e] (°)
diol-2Me-[1,1][2]PCP	1.41	1.41	—[f]	111.05	101.45
2diols-[1,1][2]PCP	1.41	1.41	—[f]	111.74	101.20
2diols-[1,1][3]PCP	1.42	1.41	—[f]	110.55	104.03
2ketones-[1,1][4]PCP	—[f]	—[f]	1.22	—[f]	113.19

[a] Define as the C–O bond lengths d_1. [b] Define as the C–O bond lengths d_2. [c] The C=O bond lengths of the carbonyl group in the macrocyclic diketones. [d] Define α_1 as the exocyclic O–C–O bond angle. [e] Define α_2 as the intracyclic C–C–C bond angle. [f] Not applicable.

Thermal stability of the macrocyclic *gem*-diols

The thermal stability of **2diols-[1.1][2]PCP**, **2diols-[1.1][3]PCP**, and **diol-2Me-[1.1][2]PCP** was evaluated by thermogravimetric analysis (TGA). The powders of **2diols-[1.1][2]PCP**, **2diols-[1.1][3]PCP**, and **diol-2Me-[1.1][2]PCP** used for TGA were prepared by recrystallization from ethyl acetate/*n*-hexane, followed by vacuum drying for 24 hours. As shown in Fig. 4, **2diols-[1.1][2]PCP** (black line) exhibited no weight loss until 150 °C. Then, between 150 °C and 210 °C, an approximate 8% weight loss was observed, corresponding to the release of two water molecules. Upon continued heating above 205 °C, the sample gradually underwent complete decomposition. The results implied that, although **2diols-[1.1][2]PCP** could dehydrate and likely form **2ketones-[1.1][2]PCP**, the latter is not sufficiently stable to be isolated. This observation is consistent with the results of the heating experiments on **2diols-[1.1][2]PCP** mentioned above.

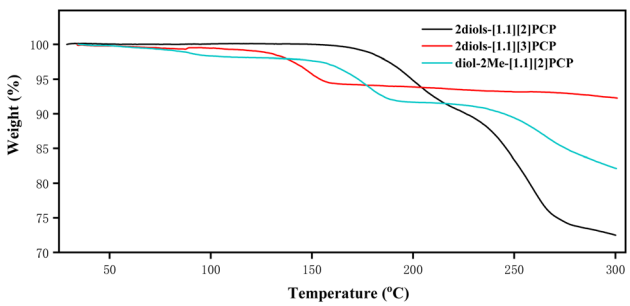

Fig. 4 Thermogravimetric analysis of **2diols-[1,1][2]PCP**, **2diols-[1,1][3]PCP** and **diol-2Me-[1,1][2]PCP**, measured under nitrogen atmosphere.

For **diol-2Me-[1.1][2]PCP** (Fig. 4, cyan line), an initial approximate 2% weight loss from 30 °C to 110 °C was observed, which can be attributed to the loss of solvent molecules engaged in hydrogen bonding with the geminal diols. Between 140 °C and 190 °C, an approximate 6% weight loss may be attributed to the release of a water molecule. In the case of **2diols-[1.1][3]PCP** (Fig. 4, green line), a weight loss of approximately 4% between 100 °C and 160 °C corresponds to the elimination of two water molecules. Above 160 °C, the TGA curve exhibited a distinct plateau, indicating the formation of **2ketones-[1.1][3]PCP**. **2ketones-[1.1][3]PCP** remained thermally stable over a broad temperature range, consistent with the dehydration experiments described in the synthesis section.

TGA measurements indicate that **2diols-[1.1][2]PCP** is more thermally stable than **diol-2Me-[1.1][2]PCP**, which may be attributed to the more extensive intermolecular hydrogen-bonding network present in **2diols-[1.1][2]PCP**. **2diols-[1.1][2]PCP** and **diol-2Me-[1.1][2]PCP** exhibit greater thermal stability than **2diols-[1.1][3]PCP**. These results, along with the observation that acid hydrolysis of **2ketals-[1.1][4]PCP** did not yield the macrocyclic geminal diol product, suggest that the stability of macrocyclic geminal diols depends on ring size; specifically, increasing the ring size leads to reduced thermal stability. This trend is likely attributed to the reduction of angular strain in larger macrocycles, which renders the geminal diol functionality less thermodynamically favored.

DFT calculation

To further elucidate the structure–stability relationships, gas-phase geometry optimizations and strain energy calculations[60–62] were performed at the WB97XD/6-311G(d) level for macrocyclic *gem*-diols—including **diol-2Me-[1,1][2]PCP** and **2diols-[1,1][*n*]PCPs**—their corresponding macrocyclic diketones (**ketone-2Me-[1,1][2]PCP** and **2ketones-[1,1][*n*]PCPs**), and the respective macrocyclic ketals (**ketal-2Me-[1,1][2]PCP** and **2ketals-[1,1][*n*]PCPs**) (See SI, Fig. S74). The optimized core structures are in good agreement with the corresponding single-crystal X-ray structures (Table 3).

The strain energies of **2diols-[1.1][2]PCP**, **2diols-[1.1][3]PCP**, and **2diols-[1.1][4]PCP** were calculated to be 45.33, 31.33, and 26.12 kcal mol^{-1}, respectively, whereas those of **2ketones-[1.1][2]PCP**, **2ketones-[1.1][3]PCP**, and **2ketones-[1.1][4]PCP** were 68.94, 52.98, and 46.40 kcal mol^{-1}, respectively. In all three comparisons the strain energies of the *gem*-diol forms are more than 20 kcal mol^{-1} lower than those of the corresponding ketone forms. The strain energy of **diol-2Me-[1.1][2]PCP** is 11.55 kcal mol^{-1} lower than that of **ketone-2Me-[1.1][2]PCP**; this difference is approximately half of the aforementioned strain energy gaps, consistent with the fact that **diol-2Me-[1.1][2]PCP** contains only one *gem*-diol moiety. The strain energies of the macrocyclic ketals are similar to those of the corresponding macrocyclic *gem*-diols but are lower than those of the corresponding macrocyclic diketones.

The calculated internal angles for **2diols-[1.1][2]PCP**, **2diols-[1.1][3]PCP**, and **2diols-[1.1][4]PCP** are 101.82°, 103.65°, and 105.96°, respectively, which are smaller than those of the corresponding diketones (**2ketones-[1.1][2]PCP**, **2ketones-[1.1][3]PCP**, **2ketones-[1.1][4]PCP**: 104.23°, 108.58°, 112.71°, respectively). The calculated internal angles of the ketals (**2ketals-[1.1][2]PCP**, **2ketals-[1.1][3]PCP**, **2ketals-[1.1][4]PCP**) are 101.86°, 102.74°, and 104.10°, respectively, showing an increasing trend with macrocycle size that aligns well with single-crystal X-ray data. On the basis of these computational and experimental results, we propose that the calculated internal angle of macrocyclic diketones can be used as a predictive indicator of relative stability: for internal angles ≈ 108° both ketone and *gem*-diol forms may be thermodynamically accessible; for internal angles ≤ 104° the *gem*-diol form is strongly favored; and for internal angles ≥ 112° the ketone form is strongly favored.

We compared the strain distribution of **2diols-[1,1][*n*]PCPs** (n = 2, 3, 4) and **2ketones-[1,1][*n*]PCPs** (n = 2, 3, 4) by strain

Table 3 Summary of the physical properties of macrocyclic *gem*-diols

Entry	Compound	Strain energy (kcal mol^{-1})	The inner angle (°)
1	**ketal-2Me-[1,1][2]PCP**	50.29	100.97
	diol-2Me-[1,1][2]PCP	45.96	101.86
	ketone-2Me-[1,1][2]PCP	57.51	104.11
2	**2ketals-[1,1][2]PCP**	43.89	100.90
	2diols-[1,1][2]PCP	45.33	101.82
	2ketones-[1,1][2]PCP	68.94	104.23
3	**2ketals-[1,1][3]PCP**	29.64	102.74
	2diols-[1,1][3]PCP	31.33	103.65
	2ketone-[1,1][3]PCP	52.98	108.58
4	**2ketals-[1,1][4]PCP**	25.70	104.10
	2diols-[1,1][4]PCP	26.12	105.96
	2ketones-[1,1][4]PCP	46.40	112.71

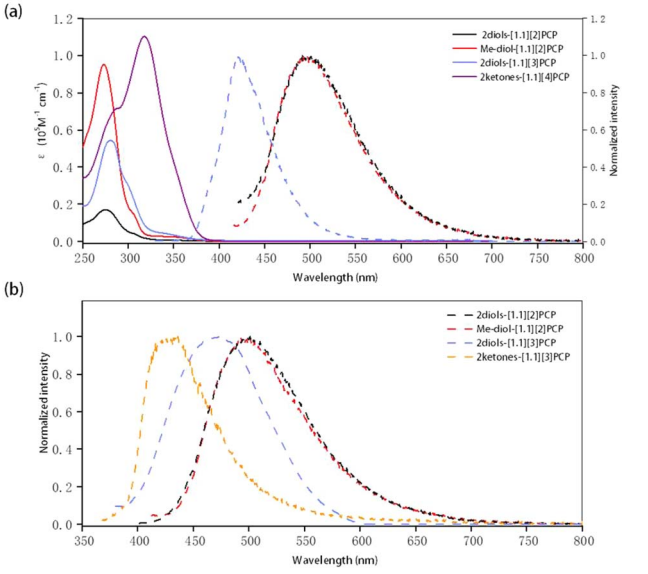

Fig. 5 (a) UV-visible absorption (solid line) and fluorescence spectra (dashed line) of 2Me-diol-[1,1][2]PCP, 2diols-[1,1][2]PCP, 2diols-[1,1][3]PCP and 2ketones-[1,1][4]PCP in THF. (b) PL spectra of 2Me-diol-[1,1][2]PCP, 2diols-[1,1][2]PCP, 2diols-[1,1][3]PCP and 2ketones-[1,1][3]PCP in solid state.

Table 4 Summary of the photophysical properties of macrocyclic *gem*-diols and macrocyclic diketones

Compound	λ_{abs}[a] (nm)	$\lambda_{PL,s}$[b] (nm)	$\lambda_{PL,sl}$[c] (nm)	$\Phi_{PL,s}$[d] (%)	$\Phi_{PL,sl}$[e] (%)
diol-Me-[1,1][2]PCP	273	503.5	491.5	10.13	12.73
2diols-[1,1][2]PCP	274	501	491.5	17.74	6.92
2diols-[1,1][3]PCP	280	425.5	420.5	20.55	38.23
2ketones-[1,1][3]PCP	—	474	—	6.72	—
2ketones-[1,1][4]PCP	317	—	—	—	—

[a] UV-visible maximum absorption in THF solution. [b] PL maximum in solid state. [c] PL maximum in THF solution. [d] Absolute photoluminescence quantum yield in solid state. [e] Absolute photoluminescence quantum yield in THF solution.

visualization using StrainViz.[63] For **2diols-[1,1][*n*]PCPs** ($n = 2$, 3, 4) and **2ketones-[1,1][*n*]PCPs**, the highest strain energy is located at the C_{phenyl}–$C_{gem\text{-}diol}$ and C_{phenyl}–$C_{carbonyl}$ bonds, respectively (see SI, Fig. S84). The highest strain energies in **2ketones-[1,1][*n*]PCPs** are approximately 1.5 to 2.5 times higher than those in the corresponding **2diols-[1,1][*n*]PCPs**.

These results indicate that an increase in macrocycle size leads to a pronounced decrease in ring strain energy, while dehydration of *gem*-diols to the corresponding sp^2-hybridized carbonyl compounds significantly increases the ring strain energy across different macrocycle sizes. Thus, from the perspective of ring strain energy, the formation of geminal diols within strained macrocyclic frameworks enhances stability.

Photophysical properties

The UV-vis absorption properties of these macrocycles in dilute THF solution were investigated, and the results are presented in Fig. 5, Tables 4 and S24. The absorption bands of the macrocyclic *gem*-diols, attributed to π–π* electronic transitions, were observed in the range of 273 to 280 nm. A distinct redshift in the maximum absorption wavelengths was observed with increasing macrocycle size, which is likely due to the extended conjugation of biphenyl units as the ring size increases. For macrocyclic diketones, the maximum absorption wavelength (λ_{max}) of **2ketones-[1.1][4]PCP** was measured to be 317 nm. However, due to the rapid conversion of **2ketones-[1.1][3]PCP** to **2diols-[1.1][3]PCP** in THF, the photophysical properties of **2ketones-[1.1][3]PCP** could not be obtained in this solvent.

These macrocyclic *gem*-diols exhibit strong fluorescence in both THF solution and the solid state. In THF solution, the maximum emission wavelengths ($\lambda_{PL,sl}$) of **2diols-[1.1][2]PCP**, **diol-2Me-[1.1][2]PCP**, and **2diols-[1.1][3]PCP** were determined to be 491.5 nm, 491.5 nm, and 420.5 nm, respectively, comparable to those of their corresponding ketal precursors (see SI). A blueshift in emission was observed with increasing macrocycle size, likely due to the relaxation of ring strain. The photoluminescence quantum yields ($\Phi_{PL,sl}$) of **2diols-[1.1][2]PCP**, **diol-2Me-[1.1][2]PCP**, and **2diols-[1.1][3]PCP** in THF were 6.92%, 12.73%, and 38.23%, respectively. Similar to their behavior in THF, **2diols-[1.1][2]PCP**, **diol-2Me-[1.1][2]PCP**, and **2diols-[1.1][3]PCP** exhibit solid-state maximum emission wavelengths ($\lambda_{PL,s}$) of 501 nm, 503.5 nm, and 425.5 nm, respectively. Their corresponding solid-state $\Phi_{PL,s}$ values were 17.74%, 10.13%, and 20.55%. For macrocyclic diketones, no visible emission was detected for **2ketones-[1.1][4]PCP**. In contrast, **2ketones-[1.1][3]PCP** exhibits solid-state emission with a maximum emission wavelength of 474 nm and a $\Phi_{PL,s}$ of 6.72%. Such shifts and changes in quantum yields may be attributed to alterations in conjugation length and ring strain, which modulate the electronic structures and non-radiative decay pathways of these macrocycles.

Conclusion

In summary, a series of crystalline, stable, and rigid macrocyclic *gem*-diols and macrocyclic diketones were successfully synthesized *via* acid hydrolysis of macrocyclic ketals at −25 °C. Single-crystal X-ray diffraction analysis of **2diols-[1.1][2]PCP**, **2diols-[1.1][3]PCP**, and **diol-2Me-[1.1][2]PCP** reveals O–C–O bond angles of approximately 111°. Notably, these macrocycles form a robust eight-membered hydrogen-bonded structure in the solid state, which likely contributes to their ordered packing and enhanced stability. Thermogravimetric analysis reveals a clear, ring size-dependent thermal stability. **2diols-[1.1][2]PCP** remains stable up to 150 °C, and **diol-2Me-[1.1][2]PCP** begins to dehydrate at around 140 °C. **2diols-[1.1][3]PCP** starts to dehydrate at approximately 100 °C, whereas **2diols-[1.1][4]PCP** could not be obtained under similar conditions. The strain energies of macrocyclic *gem*-diols are consistently lower than those of their dehydrated ketone counterparts. This difference can be attributed to the sp^3-hybridized *gem*-diol carbon atoms, which better accommodate angular strain than the planar sp^2-hybridized carbons in the ketones. We propose that the calculated inner angles of macrocyclic ketones can be used to assess the relative stability of macrocyclic ketones *versus* their *gem*-diol forms. The successful synthesis of this new class of macrocyclic geminal diols not only expands the library of stable *gem*-diol compounds but also provides deeper insights into the structural features and stability factors of this important functional group, thereby laying a solid foundation for the design and synthesis of more diverse macrocyclic *gem*-diol molecules.

Author contributions

H.-W. Jiang initiated and designed the project. Supervision of the research was provided by H.-W. Jiang, B. Xu, and J. Fan. B. Zou performed the primary experiments and conducted corresponding data analysis. X. Chen contributed to part of the experimental work. H. Wei was responsible for the majority of

the photophysical measurements. H. Liu, S. Wen, and J. Huang aided in data collection and analysis. The initial draft of the manuscript was prepared by B. Zou. All authors participated in the discussion and revision of the manuscript.

Conflicts of interest

The authors declare no competing financial interests.

Data availability

CCDC 2479706 (**diol-2Me-[1.1][2]PCP**), 2479718 (**2diols-[1.1][2]PCP**), 2479720 (**2diols-[1.1][3]PCP**), 2479725 (**2ketones-[1.1][4]PCP**), 2479728 (**2dbts-[1.1][2]PCP**), 2479740 (**ketal-2Me-[1.1][2]PCP**), 2479742 (**2ketals-[1.1][4]PCP**), 2479743 (**2ketals-[1.1][2]PCP**) and 2479744 (**2ketals-[1.1][3]PCP**) contain the supplementary crystallographic data for this paper.[64a–i]

Supplementary information: experimental procedures, characterization data for compounds, NMR spectra, thermogravimetric analysis, and X-ray crystallographic data. See DOI: https://doi.org/10.1039/d5sc08216a.

Acknowledgements

This work was supported by the Natural Science Foundation of Guangdong Province, China (grant no. 2022A1515012199) and the 2022 Guangdong–Hong Kong–Macao Greater Bay Area Exchange Programs of South China Normal University. The authors gratefully acknowledge Prof. Ji-Chang Xiao and Prof. Xiaopeng Li at the Shanghai Institute of Organic Chemistry, Chinese Academy of Sciences, and Prof. Jianxin Song at the College of Chemistry and Chemical Engineering of Hunan Normal University for their assistance with MALDI-TOF mass spectrometry measurements.

Notes and references

1 J.-J. Li, C. Li, C. A. Blindauer and T. D. H. Bugg, Evidence for a *gem*-Diol Reaction Intermediate in Bacterial C–C Hydrolase Enzymes BphD and MhpC from ^{13}C NMR Spectroscopy, *Biochemistry*, 2006, **45**, 12461–12469.

2 F. K. Yoshimoto and F. P. Guengerich, Mechanism of the Third Oxidative Step in the Conversion of Androgens to Estrogens by Cytochrome P450 19A1 Steroid Aromatase, *J. Am. Chem. Soc.*, 2014, **136**, 15016–15025.

3 K. Xu, Y. Wang and H. Hirao, Estrogen Formation *via* H-Abstraction from the O–H Bond of *gem*-Diol by Compound I in the Reaction of CYP19A1: Mechanistic Scenario Derived from Multiscale QM/MM Calculations, *ACS Catal.*, 2015, **5**, 4175–4179.

4 E. G. Kovaleva and J. D. Lipscomb, Intermediate in the O–O Bond Cleavage Reaction of an Extradiol Dioxygenase, *Biochemistry*, 2008, **47**, 11168–11170.

5 G. J. Christian, S. Ye and F. Neese, Oxygen activation in extradiol catecholate dioxygenases–a density functional study, *Chem. Sci.*, 2012, **3**, 1600–1611.

6 B. Franco, T. Blumenstock, C. Cho, L. Clarisse, C. Clerbaux, P. F. Coheur, M. De Mazière, I. De Smedt, H. P. Dorn, T. Emmerichs, H. Fuchs, G. Gkatzelis, D. W. T. Griffith, S. Gromov, J. W. Hannigan, F. Hase, T. Hohaus, N. Jones, A. Kerkweg, A. Kiendler-Scharr, E. Lutsch, E. Mahieu, A. Novelli, I. Ortega, C. Paton-Walsh, M. Pommier, A. Pozzer, D. Reimer, S. Rosanka, R. Sander, M. Schneider, K. Strong, R. Tillmann, M. Van Roozendael, L. Vereecken, C. Vigouroux, A. Wahner and D. Taraborrelli, Ubiquitous atmospheric production of organic acids mediated by cloud droplets, *Nature*, 2021, **593**, 233–237.

7 A. Parandaman, M. Kumar, J. S. Francisco and A. Sinha, Organic acid formation from the atmospheric oxidation of gem diols: Reaction mechanism, energetics, and rates, *J. Phys. Chem. A*, 2018, **122**, 6266–6276.

8 J. L. Axson, K. Takahashi, D. O. De Haan and V. Vaida, Gas-phase water-mediated equilibrium between methylglyoxal and its geminal diol, *Proc. Natl. Acad. Sci. U. S. A.*, 2010, **107**, 6687–6692.

9 Z.-Z. Xie, Y. Zheng, C.-P. Yuan, J.-P. Guan, Z.-P. Ye, J.-A. Xiao, H.-Y. Xiang, K. Chen, X.-Q. Chen and H. Yang, Photoredox-Catalyzed Deoxygenation of Hexafluoroacetone Hydrate Enables Hydroxypolyfluoroalkylation of Alkenes, *Angew. Chem., Int. Ed.*, 2022, **61**, e202211035.

10 H. A. Rypkema, A. Sinha and J. S. Francisco, Carboxylic Acid Catalyzed Hydration of Acetaldehyde, *J. Phys. Chem. A*, 2015, **119**, 4581–4588.

11 A. Das, S. Mahale, V. Prashar, S. Bihani, J. L. Ferrer and M. V. Hosur, X-ray Snapshot of HIV-1 Protease in Action: Observation of Tetrahedral Intermediate and Short Ionic Hydrogen Bond SIHB with Catalytic Aspartate, *J. Am. Chem. Soc.*, 2010, **132**, 6366–6373.

12 A. Krzemińska, V. Moliner and K. Świderek, Dynamic and Electrostatic Effects on the Reaction Catalyzed by HIV-1 Protease, *J. Am. Chem. Soc.*, 2016, **138**, 16283–16298.

13 L. Bravo-García, G. Barandika, B. Bazán, M. K. Urtiaga and M. I. Arriortua, Thermal stability of ionic nets with Cu^{II} ions coordinated to di-2-pyridyl ketone: Reversible crystal-to-crystal phase transformation, *Polyhedron*, 2015, **92**, 117–123.

14 C. G. Efthymiou, C. P. Raptopoulou, V. Psycharis, A. J. Tasiopoulos, A. Escuer, S. P. Perlepes and C. Papatriantafyllopoulou, Copper(II)/di-2-pyridyl ketone chemistry: A triangular cluster displaying antisymmetric exchange *versus* an 1D coordination polymer, *Polyhedron*, 2013, **64**, 30–37.

15 G. Yang, M.-L. Tong, X.-M. Chen and S. W. Ng, Bis(di-2-pyridylmethanediol-*N,O,N'*)copper(II) Diperchlorate, *Acta Crystallogr., Sect. C:Cryst. Struct. Commun.*, 1998, **54**, 732–734.

16 D. G. Mantero, M. Altaf, A. Neels and H. Stoeckli-Evans, Pyridin-4-ylmethanediol: the hydrated form of isonicotinaldehyde, *Acta Crystallogr., Sect. E:Struct. Rep. Online*, 2006, **62**, o5204–o5206.

17 D. P. Giannopoulos, L. Cunha-Silva, R. Ballesteros-Garrido, R. Ballesteros, B. Abarca, A. Escuer and T. C. Stamatatos, New structural motifs in Mn cluster chemistry from the

ketone/*gem*-diol and bis(*gem*-diol) forms of 2,6-di-(2-pyridylcarbonyl)pyridine: {$Mn^{II}_4Mn^{III}_2$} and {$Mn^{II}_4Mn^{III}_6$} complexes, *RSC Adv.*, 2016, **6**, 105969–105979.

18 H.-S. Wang, F.-J. Yang, Q.-Q. Long, Z.-Y. Huang, W. Chen and Z.-Q. Pan, Syntheses, crystal structures, and magnetic properties of a family of heterometallic octanuclear [Cu_6Ln_2] (Ln = Dy(iii), Tb(iii), Ho(iii), Er(iii), and Gd(iii)) complexes, *New J. Chem.*, 2017, **41**, 5884–5892.

19 T. C. Stamatatos, V. Nastopoulos, A. J. Tasiopoulos, E. E. Moushi, W. Wernsdorfer, G. Christou and S. P. Perlepes, High Nuclearity Single-Molecule Magnets: a Mixed-Valence Mn_{26} Cluster Containing the Di-2-pyridylketone Diolate Dianion, *Inorg. Chem.*, 2008, **47**, 10081–10089.

20 A. J. Tasiopoulos and S. P. Perlepes, Diol-type ligands as central 'players' in the chemistry of high-spin molecules and single-molecule magnets, *Dalton Trans.*, 2008, 5537–5555.

21 K. B. Wiberg, K. M. Morgan and H. Maltz, Thermochemistry of Carbonyl Reactions. 6. A Study of Hydration Equilibria, *J. Am. Chem. Soc.*, 1994, **116**, 11067–11077.

22 C. Zhu, N. F. Kleimeier, A. M. Turner, S. K. Singh, R. C. Fortenberry and R. I. Kaiser, Synthesis of methanediol [$CH_2(OH)_2$]: The simplest geminal diol, *Proc. Natl. Acad. Sci. U. S. A.*, 2022, **119**, e2111938119.

23 M. S. Yu, *gem*-Polyols — a unique class of compound, *Russ. Chem. Rev.*, 1991, **60**, 1035.

24 J. M. Lázaro Martínez, P. N. Romasanta, A. K. Chattah and G. Y. Buldain, NMR Characterization of Hydrate and Aldehyde Forms of Imidazole-2-carboxaldehyde and Derivatives, *J. Org. Chem.*, 2010, **75**, 3208–3213.

25 A. F. Crespi and J. M. Lázaro-Martínez, Can a *gem*-Diol Moiety Be Isolated? A Reaction Study by NMR and X-ray Spectroscopies, *J. Chem. Educ.*, 2023, **100**, 4536–4542.

26 A. F. Crespi, A. J. Byrne, D. Vega, A. K. Chattah, G. A. Monti and J. M. Lázaro-Martínez, Generation and Stability of the *gem*-Diol Forms in Imidazole Derivatives Containing Carbonyl Groups. Solid-State NMR and Single-Crystal X-ray Diffraction Studies, *J. Phys. Chem. A*, 2018, **122**, 601–609.

27 A. F. Crespi, D. Vega, A. K. Chattah, G. A. Monti, G. Y. Buldain and J. M. Lázaro-Martínez, *gem*-Diol and Hemiacetal Forms in Formylpyridine and Vitamin-B_6-Related Compounds: Solid-State NMR and Single-Crystal X-ray Diffraction Studies, *J. Phys. Chem. A*, 2016, **120**, 7778–7785.

28 F. I. Luknitskii, Chemistry of chloral, *Chem. Rev.*, 1975, **75**, 259–289.

29 D. J. McCaldin, The Chemistry of Ninhydrin, *Chem. Rev.*, 1960, **60**, 39–51.

30 P. Lipp, J. Buchkremer and H. Seeles, Studien in der Cyclopropan-Reihe. Cyclo-propanon, *Adv. Cycloaddit.*, 1932, **499**, 1–25.

31 S. E. Schaafsma, H. Steinberg and T. J. de Boer, The chemistry of cyclopropanones. Part VI: Addition of 1,1-dihydroxycyclopropane, *Recl. Trav. Chim. Pays-Bas*, 1967, **86**, 651–654.

32 P. Zuman, Additions of water, hydroxyde ion, alcohols and alkoxide ions to carbonyl and azomethine bonds, *Arkivoc*, 2002, **1**, 85–140.

33 H. Cui, R. Goddard, K.-R. Pörschke, A. Hamacher and M. U. Kassack, Bispidin-9,9-diol Analogues of Cisplatin, Carboplatin, and Oxaliplatin: Synthesis, Structures, and Cytotoxicity, *Inorg. Chem.*, 2016, **55**, 2986–2997.

34 K. Bleher, P. Comba, M. Gast, S. Kronenberger and T. Josephy, Copper-bispidine-catalyzed aziridination–A new twist in small molecule activation, *Inorg. Chim. Acta*, 2022, **532**, 120752.

35 S. E. Lewis, Cycloparaphenylenes and related nanohoops, *Chem. Soc. Rev.*, 2015, **44**, 2221–2304.

36 H. Kono, Y. Li, R. Zanasi, G. Monaco, F. F. Summa, L. T. Scott, A. Yagi and K. Itami, Methylene-Bridged [6]-, [8]-, and [10]Cycloparaphenylenes: Size-Dependent Properties and Paratropic Belt Currents, *J. Am. Chem. Soc.*, 2023, **145**, 8939–8946.

37 H. Shudo, M. Kuwayama, M. Shimasaki, T. Nishihara, Y. Takeda, N. Mitoma, T. Kuwabara, A. Yagi, Y. Segawa and K. Itami, Perfluorocycloparaphenylenes, *Nat. Commun.*, 2022, **13**, 3713.

38 Y. Han, S. Wu, K. Y. S. Khoo and C. Chi, Synthesis of fully π-conjugated non-alternant carbon nanobelts, *Nat. Synth.*, 2025, **4**, 947–955.

39 N. Narita, Y. Kurita, K. Osakada, T. Ide, H. Kawai and Y. Tsuchido, A dodecamethoxy [6] cycloparaphenylene consisting entirely of hydroquinone ethers: unveiling in-plane aromaticity through a rotaxane structure, *Nat. Commun.*, 2023, **14**, 8091.

40 K. Y. Cheung, K. Watanabe, Y. Segawa and K. Itami, Synthesis of a zigzag carbon nanobelt, *Nat. Chem.*, 2021, **13**, 255–259.

41 T. D. Clayton, J. M. Fehr, T. W. Price, L. N. Zakharov and R. Jasti, Pinwheel-like Curved Aromatics from the Cyclotrimerization of Strained Alkyne Cycloparaphenylenes, *J. Am. Chem. Soc.*, 2024, **146**, 30607–30614.

42 P. C. Hall, H. W. Reid, I. Liashenko, B. Tandon, K. L. O'Neill, N. C. Paxton, G. C. J. Lindberg, R. Jasti and P. D. Dalton, [*n*] Cycloparaphenylenes as compatible fluorophores for melt electrowriting, *Small*, 2024, **20**, 2400882.

43 A. A. Kamin, T. D. Clayton, C. E. Otteson, P. M. Gannon, S. Krajewski, W. Kaminsky, R. Jasti and D. J. Xiao, Synthesis and metalation of polycatechol nanohoops derived from fluorocycloparaphenylenes, *Chem. Sci.*, 2023, **14**, 9724–9732.

44 E. J. Leonhardt and R. Jasti, Emerging applications of carbon nanohoops, A Donor–Acceptor 10-Cycloparaphenylene and Its Use as an Emitter in an Organic Light-Emitting Diode, *Nat. Rev. Chem.*, 2019, **3**, 672–686.

45 D. Chen, Y. Wada, Y. Kusakabe, L. Sun, E. Kayahara, K. Suzuki, H. Tanaka, S. Yamago, H. Kaji and E. Zysman-Colman, *Org. Lett.*, 2023, **25**, 998–1002.

46 T. Terabayashi, E. Kayahara, Y. Zhang, Y. Mizuhata, N. Tokitoh, T. Nishinaga, T. Kato and S. Yamago, Synthesis

of twisted [N] cycloparaphenylene by alkene insertion, *Angew. Chem., Int. Ed.*, 2023, **135**, e202214960.

47 Y. Yoshigoe, Y. Tanji, Y. Hata, K. Osakada, S. Saito, E. Kayahara, S. Yamago, Y. Tsuchido and H. Kawai, Dynamic Au–C σ-Bonds Leading to an Efficient Synthesis of [*n*]Cycloparaphenylenes (n = 9–15) by Self-Assembly, *JACS Au*, 2022, **2**, 1857–1868.

48 Y. Miyazawa, Z. Wang, M. Matsumoto, S. Hatano, I. Antol, E. Kayahara, S. Yamago and M. Abe, 1,3-Diradicals Embedded in Curved Paraphenylene Units: Singlet *versus* Triplet State and In-Plane Aromaticity, *J. Am. Chem. Soc.*, 2021, **143**, 7426–7439.

49 A. Usami, H. Kono, V. Austen, Q. M. Phung, H. Shudo, T. Kato, H. Yamada, A. Yagi, K. Amaike, K. J. Fujimoto, T. Yanai and K. Itami, In-insect synthesis of oxygen-doped molecular nanocarbons, *Science*, 2025, **388**, 1055–1061.

50 B. Zou, J.-A. Li, Z. Zhai, T. Yu, H. Liu, J. Huang, H. He, B. Xu and H.-W. Jiang, *cis*-Linked Cyclotetraphenylenes: Synthesis, Structures and Fluorescence Properties, *Eur. J. Org Chem.*, 2024, **27**, e202400135.

51 H.-W. Jiang, T. Tanaka, H. Mori, K. H. Park, D. Kim and A. Osuka, Cyclic 2,12-Porphyrinylene Nanorings as a Porphyrin Analogue of Cycloparaphenylenes, *J. Am. Chem. Soc.*, 2015, **137**, 2219–2222.

52 H.-W. Jiang, T. Tanaka, T. Kim, Y. M. Sung, H. Mori, D. Kim and A. Osuka, Synthesis of [*n*]Cyclo-5,15-porphyrinylene-4,4′-biphenylenes Displaying Size-Dependent Excitation-Energy Hopping, *Angew. Chem.*, 2015, **127**, 15412–15416.

53 S. Idrees, Z. Li, F. Fang, H. He, I. Majeed, Y. Zhang, A. Osuka, Y. Cao, Z. Zeng, X. Li and H.-W. Jiang, Porphyrin nanotubes based on a hydrogen-bonded organic framework, *Nanoscale*, 2022, **14**, 14630–14635.

54 H. He, J.-A. Li, Y. Zhang, S. Idrees, J. Cai, Y. Li, A. Osuka, B. Xu and H.-W. Jiang, Synthesis, structures and fluorescence properties of *gem*-linked cyclic tetraphenylethylenes and cyclic hexaphenylethylenes, *Org. Chem. Front.*, 2022, **9**, 2932–2938.

55 E. Kayahara, S. Hirata, Y. Mizuhata, Y. Yasuda, Y. Kusakabe, H. Kaji and S. Yamago, Synthesis of π-Extended [1.1] Paracyclophanes, [1.1][n]PCP (n=2, 3, and 4), and Their Through-Space Conjugation, *Chem.–Eur. J.*, 2025, **31**, e202402225.

56 E. Kayahara, T. Hayashi, K. Takeuchi, F. Ozawa, K. Ashida, S. Ogoshi and S. Yamago, Strain-Induced Double Carbon–Carbon Bond Activations of Cycloparaphenylenes by a Platinum Complex: Application to the Synthesis of Cyclic Diketones, *Angew. Chem., Int. Ed.*, 2018, **57**, 11418–11421.

57 G. Mlostoń, M. Jasiński, A. Linden and H. Heimgartner, Reactions of 2-Unsubstituted 1*H*-Imidazole 3-Oxides with 2,2-Bis(trifluoromethyl)ethene-1,1-dicarbonitrile: A Stepwise 1,3-Dipolar Cycloaddition, *Helv. Chim. Acta*, 2006, **89**, 1304–1316.

58 E. T. Urbansky, Carbinolamines and Geminal Diols in Aqueous Environmental Organic Chemistry, *J. Chem. Educ.*, 2000, **77**, 1644.

59 H. Kutzke, H. Klapper, R. B. Hammond and K. J. Roberts, Metastable [beta]-phase of benzophenone: independent structure determinations *via* X-ray powder diffraction and single crystal studies, *Acta Crystallogr., Sect. C:Cryst. Struct. Commun.*, 2000, **56**, 486–496.

60 Y. Segawa, H. Omachi and K. Itami, Theoretical Studies on the Structures and Strain Energies of Cycloparaphenylenes, *Org. Lett.*, 2010, **12**, 2262–2265.

61 S. M. Bachrach and D. Stück, DFT Study of Cycloparaphenylenes and Heteroatom-Substituted Nanohoops, *J. Org. Chem.*, 2010, **75**, 6595–6604.

62 T. Iwamoto, Y. Watanabe, Y. Sakamoto, T. Suzuki and S. Yamago, Selective and Random Syntheses of [*n*] Cycloparaphenylenes (*n* = 8–13) and Size Dependence of Their Electronic Properties, *J. Am. Chem. Soc.*, 2011, **133**, 8354–8361.

63 C. E. Colwell, T. W. Price, T. Stauch and R. Jasti, Strain visualization for strained macrocycles, *Chem. Sci.*, 2020, **11**, 3923–3930.

64 (*a*) CCDC 2479706: Experimental Crystal Structure Determination, 2025, DOI: **10.5517/ccdc.csd.cc2p7bjt**; (*b*) CCDC 2479718: Experimental Crystal Structure Determination, 2025, DOI: **10.5517/ccdc.csd.cc2p7bx6**; (*c*) CCDC 2479720: Experimental Crystal Structure Determination, 2025, DOI: **10.5517/ccdc.csd.cc2p7bz8**; (*d*) CCDC 2479725: Experimental Crystal Structure Determination, 2025, DOI: **10.5517/ccdc.csd.cc2p7c4g**; (*e*) CCDC 2479728: Experimental Crystal Structure Determination, 2025, DOI: **10.5517/ccdc.csd.cc2p7c7k**; (*f*) CCDC 2479740: Experimental Crystal Structure Determination, 2025, DOI: **10.5517/ccdc.csd.cc2p7cmy**; (*g*) CCDC 2479742: Experimental Crystal Structure Determination, 2025, DOI: **10.5517/ccdc.csd.cc2p7cp0**; (*h*) CCDC 2479743: Experimental Crystal Structure Determination, 2025, DOI: **10.5517/ccdc.csd.cc2p7cq1**; (*i*) CCDC 2479744: Experimental Crystal Structure Determination, 2025, DOI: **10.5517/ccdc.csd.cc2p7cr2**.